Title

A Magneto-Responsive Hydrogel System for the Dynamic Mechano-Modulation of Stem Cell Niche

Journal

Advanced Functional Materials, 33(12)

ISSN

1616-301X

Authors

Goodrich, Robyn

Tai, Youyi

Ye, Zuyang

et al.

Publication Date

2023-03-01

DOI

10.1002/adfm.202211288

A Magneto-Responsive Hydrogel System for the Dynamic Mechano-Modulation of Stem Cell Niche

Robyn Goodrich[1#], Youyi Tai[1#], Zuyang Ye[2], Yadong Yin[2, 3], and Jin Nam[1, 3]*

[1]Department of Bioengineering, University of California, Riverside, CA 92521, USA

[2]Department of Chemistry, University of California, Riverside, CA 92521, USA

[3]UC-KIMS Center for Innovative Materials, Riverside, CA 92521, USA

# equally contributed

* corresponding author: Jin Nam, Ph.D., jnam@engr.ucr.edu

Keywords: dynamic modulus control, hydrogel, magnetic nanorod, stem cell differentiation, mechanotransduction

Abstract:

The biophysical microenvironment of cells dynamically evolves during embryonic development, leading to defined tissue specification. A versatile and highly adaptive magneto-responsive hydrogel system composed of magnetic nanorods and a stress-responsive polymeric matrix is developed to dynamically regulate the physical stem cell niche. We utilize the anisotropic magnetic/shape factor of nanorods to maximize the strains on the polymeric network, thus regulating the hydrogel modulus in a physiologically relevant range under a minimal magnitude of the applied magnetic fields below 4.5 mT. More significantly, the pre-alignment of magnetic nanorods induces greater collective strains on the polymeric network, resulting in a superior stiffening range, over a 500% increase as compared to that with randomly oriented nanorods. The pre-alignment of nanorods also enables a fast and reversible response under a magnetic field of the opposite polarity as well as spatially controlled heterogeneity of modulus within the hydrogel by applying anisotropic magnetic fields. The mechano-modulative capability of this system is validated by a mechanotransduction model with human-induced pluripotent stem cells where the locally controlled hydrogel modulus regulates the activation of mechano-sensitive signaling mediators and subsequent stem cell differentiation. Therefore, this magneto-responsive hydrogel system provides a platform to investigate various cellular behaviors under dynamic mechanical microenvironments.

1. Introduction

Over the past decade, the clinical potential of patient-specific cell therapy has been substantially enhanced through the safe derivation and utilization of induced pluripotent stem cells (iPSCs).[1] Human iPSCs not only offer a therapeutic source for personalized regenerative medicine but also provide a cell/tissue platform to investigate human diseases without encountering ethical barriers or improperly using genetically mismatched animal-derived cells.[2] During development, it is being more realized that the physical microenvironments of stem cells among many environmental factors significantly affect their maintenance of pluripotency, differentiation behaviors, and subsequent tissue morphogenesis.[3] Specifically, it has been demonstrated in various studies of embryonic development that mechanical cues drive stem cell differentiation toward specific lineages.[4] For example, the immobilization of chick embryos using neuromuscular blocking agents results in a malformation of the skeletal system in the absence of dynamic mechanical stimulation from muscle contractions,[5] demonstrating the significance of dynamic mechanical stimulation for the development of the musculoskeletal system. Similarly, studies have also shown the involvement of biomechanical factors in the morphogenesis of various other tissues such as the brain, blood vessels, and heart.[6] These developmental studies showed that *in vivo* stem cell niches are mechanically dynamic microenvironments that continuously evolve to orchestrate cellular activities for tissue morphogenesis and homeostasis.[7] Therefore, extracellular matrix (ECM) modeling/remodeling is integral in modulating stem cell behaviors.

In order to recapitulate the physical niches for desired stem cell behaviors, i.e., differentiation towards specific lineages/phenotypes, various types of scaffolds have been utilized.[8] Among numerous platforms, hydrogel systems including mammalian cell-derived Matrigel/Geltrex, tissue-derived collagen, hybrid gelatin methacrylate (GelMA), and synthetic polymeric scaffolds, have been widely utilized due to their physicochemical similarities to the 3D microenvironments of *in vivo* ECM. However, their static nature falls short of mimicking the dynamic stem cell microenvironments, especially the continuously evolving mechanical microenvironment that guides tissue morphogenesis. Two major approaches to recapitulate the dynamic mechanical niche of cells in hydrogel systems involve one utilizing the in-situ control over crosslinking density to regulate hydrogel stiffness.[9] Jeon et al. developed a reversibly tunable alginate hydrogel that relies on calcium concentration to control the crosslinking density,

allowing for the tuning of hydrogel elastic modulus.[10] A shortfall of this approach includes a small dynamic range of modulus as well as a slower stiffening/softening rate. The other approach utilizes exogenously applied physical stimuli to control hydrogel elastic modulus such as temperature or a magnetic field. Hackelbusch et al. developed a thermo-tunable elastic hydrogel that enables reversible tuning of mechanical elasticity through temperature adjustment.[11] This method, however, is not suitable for biological systems due to the temperature sensitivity of cells and tissues. On the other hand, magnetic fields in combination with magnetic nanoparticles (MNPs) embedded within the hydrogel have shown a potential for dynamically controlling the mechanical microenvironment of cells while maintaining the proper cell culture conditions.[12] In this application, MNPs are used as a mediator, converting the applied magnetic fields to the change of hydrogel modulus by the particle motion, straining the polymeric network of the hydrogel. Recently, Yan et al. developed a magnetic nanocomposite hydrogel with tunable modulus utilizing the activation of the magnetic nanoparticles under a magnetic field, where the cells cultured on the surface of the hydrogel experienced and responded to the magnetic field-induced stiffness change of the hydrogel.[13] One shortcoming of this approach is the efficiency of magnetic energy-to-hydrogel modulus change in that high intensity of the magnetic field is required to obtain a relatively small range of modulus change, which may cause physiological and growth abnormalities of the cells cultured under such strong magnetic fields.[14] Furthermore, the reversibility of the system is questionable as the application of magnetic fields resulted in the permanent deformation of the composite hydrogel.

In this study, a magneto-responsive hydrogel system was developed by incorporating Fe_3O_4@SiO_2 magnetic nanorods (MNRs) within GelMA hydrogel, where the elastic modulus of the hydrogel can be dynamically and reversibly modulated by the application of relatively low magnetic fields (**Figure 1**). A four-electromagnet setup was utilized to simultaneously control the polarity and magnitudes of the applied magnetic fields in real time, allowing complete control over heterogeneous modulus mapping. We demonstrated that the application of magnetic fields predictably controlled the local modulus of the hydrogel due to MNR rearrangement, straining the polymeric network of the hydrogel. Furthermore, we showed that pre-aligning MNRs prior to hydrogel cross-linking substantially enhanced the dynamic range of the modulus change. Such control of the hydrogel stiffness significantly affected iPSC differentiation via the

modulation over the RhoA and YAP signaling pathways, demonstrating the potential of the magneto-responsive hydrogel system for guiding stem cell-based tissue morphogenesis.

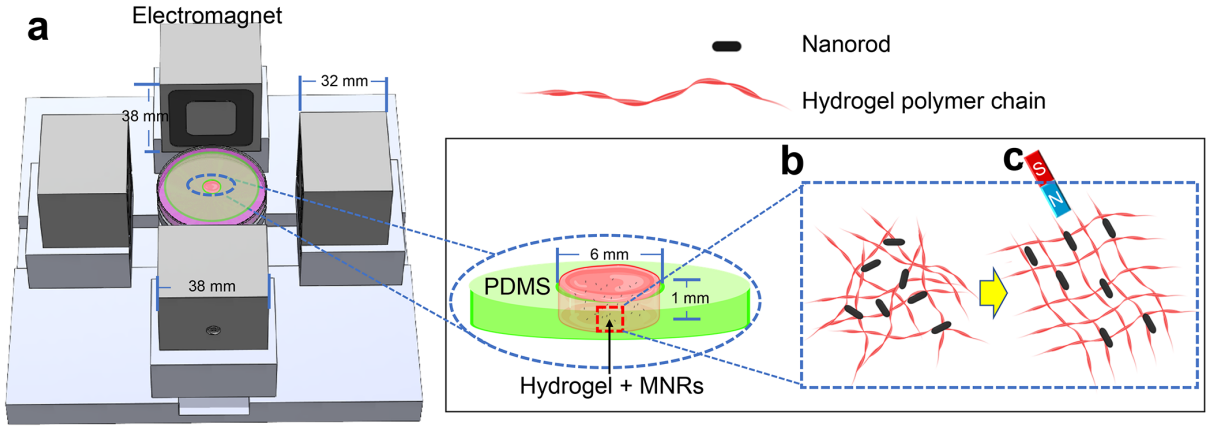

Figure 1. Schematic of a magneto-responsive hydrogel system, based on the stiffening of the hydrogel from the mechanical straining of polymer network by magnetic Fe_3O_4@SiO_2 nanorod (MNR) re-orientation under the applied magnetic fields. (a) MNR-incorporated gelatin methacrylate (GelMA) hydrogel was cast in a PDMS mold with a cylindrical well (diameter: 6 mm, height: 1 mm), which was placed in the center of four electromagnets. The four electromagnets were orthogonally placed around the hydrogel and the distance between two face-to-face electromagnets was 5 cm. (b) Randomly distributed MNRs in the hydrogel network. (c) Mechanical straining when exposed to magnetic fields (graphics are not in scale).

2. Results

The working principle of our strategy to utilize a magneto-responsive hydrogel system for the mechano-modulation of stem cell niche is based on the straining of the hydrogel polymer network by the re-arrangement of MNPs within the hydrogel under the applied magnetic fields. Therefore, the shape of the MNPs is an integral factor determining the efficiency of magnetic field-induced hydrogel stiffening. To examine the effects of the shape factor, the change in the elastic modulus of the hydrogel in response to an applied magnetic field was monitored when incorporated with either magnetic nanospheres (MNSs) or MNRs, having dimensions to occupy the same volume (**Figure 2a, b**). In order to obtain a uniform magnetic field, the optimal configuration/placement of the electromagnets was determined by COMSOL modeling. The same polarity on each electromagnet generated the magnetic field gradients to evenly align in the center of those orthogonally positioned electromagnets, where the MNP-incorporated hydrogel will be placed **(Figure 2c)**. With increasing magnetic field intensity from 0 mT up to 4.5 mT in

this electromagnet configuration, the hydrogel incorporated with MNSs exhibited a slight increase in the reduced Young's modulus from 10 kPa to 16 kPa, measured by an atomic force microscope (AFM) with a spherical tip **(Figure 2d)**. In comparison, MNR-incorporated hydrogel exhibited a modulus change from 10 kPa to 21 kPa **(Figure 2e)**, demonstrating a superior dynamic range of approximately a 2-fold increase compared to that of MNS.

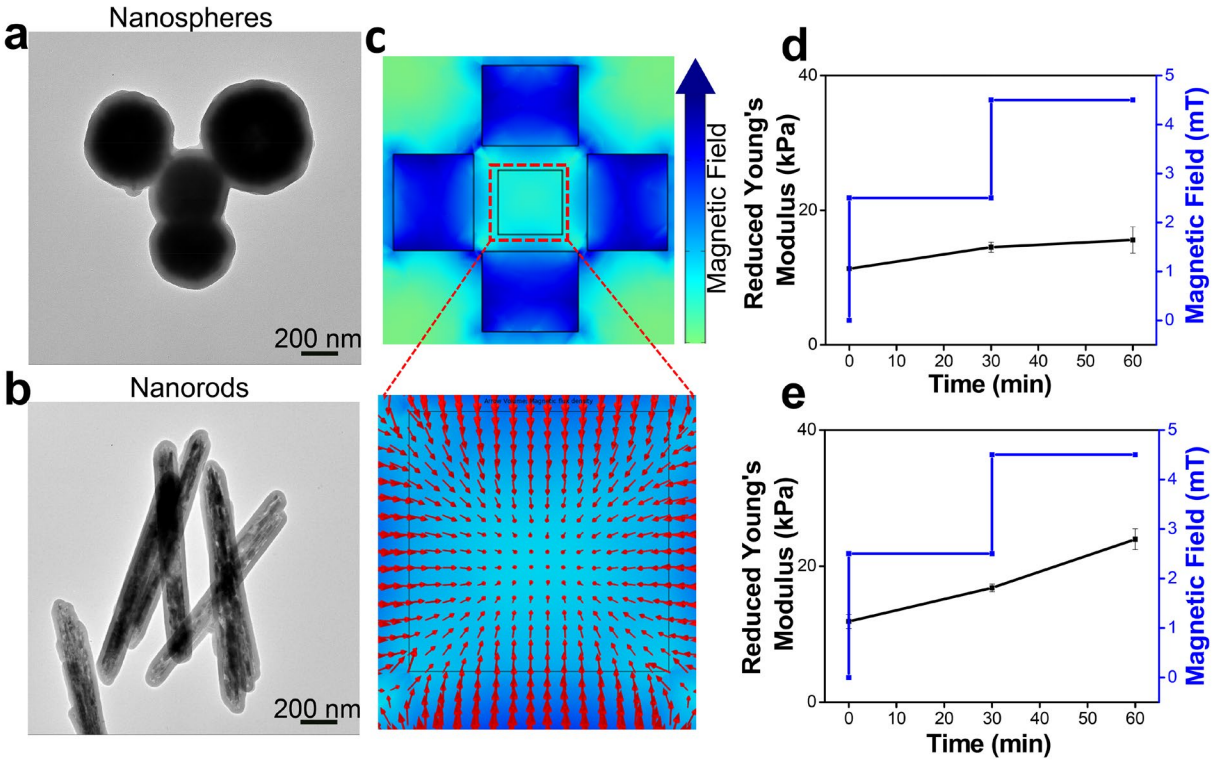

Figure 2. Transmission electron microscopy images showing the morphology of (a) magnetic nanospheres (MNSs; 340 ± 44 nm in diameter) and (b) nanorods (MNRs; 1800 ± 125 nm in length and 120 ± 19 nm in diameter), both with a 40 nm thick layer of SiO_2 coating. A total of 60 MNSs and MNRs were used for the quantification of dimensions. (c) COMSOL modeling of the magnetic field distribution near the four-electromagnet setup. Modulus change of hydrogel with (d) MNSs or (e) MNRs (20 μg/ml) when exposed to the same magnetic field magnitude (up to 4.5 mT). At least 5 samples for each condition were used for modulus measurement.

Unlike MNSs, MNRs present morphological anisotropy that may exhibit orientation dependency where the initial arrangements of individual particles would affect the overall magnitude of polymer network straining, thus hydrogel stiffness. To determine the effect of MNR alignment prior to the application of magnetic fields or pre-alignment, on the modulus change of the hydrogel under magnetic fields, the mechanical properties of hydrogel with pre-

aligned MNRs were compared to that of hydrogel with randomly oriented MNRs under various magnitudes of magnetic fields. An aligned distribution pattern of MNRs was obtained by exposing the hydrogel-MNR mixture to 7.5 mT of the magnetic field for 5 mins, after which the hydrogel was crosslinked by UV exposure **(Figure 3a, b)**. The distribution of the MNRs within the hydrogel was quantified by imaging analysis, where, as expected, MNRs predominantly aligned to the major magnetic field directions shown in **Figure 2c** (**Figure 3c, d**). Subsequent application of magnetic fields with the same polarity to this pre-alignment induced the modulus change from approximately 10 kPa to 61 kPa **(Figure 3e)**. In contrast, the hydrogel with randomly oriented MNRs exhibited an inferior dynamic modulus range from approximately 10 kPa to 21 kPa **(Figure 3e)**. The results of the lower modulus range in hydrogels with randomly oriented MNRs are likely because their random rotational/translational movements neutralize each other, reducing the overall straining of the hydrogel network. These results demonstrate the enhancement of dynamic modulus range by pre-aligning MNRs, more than 500% as compared to randomly oriented MNRs.

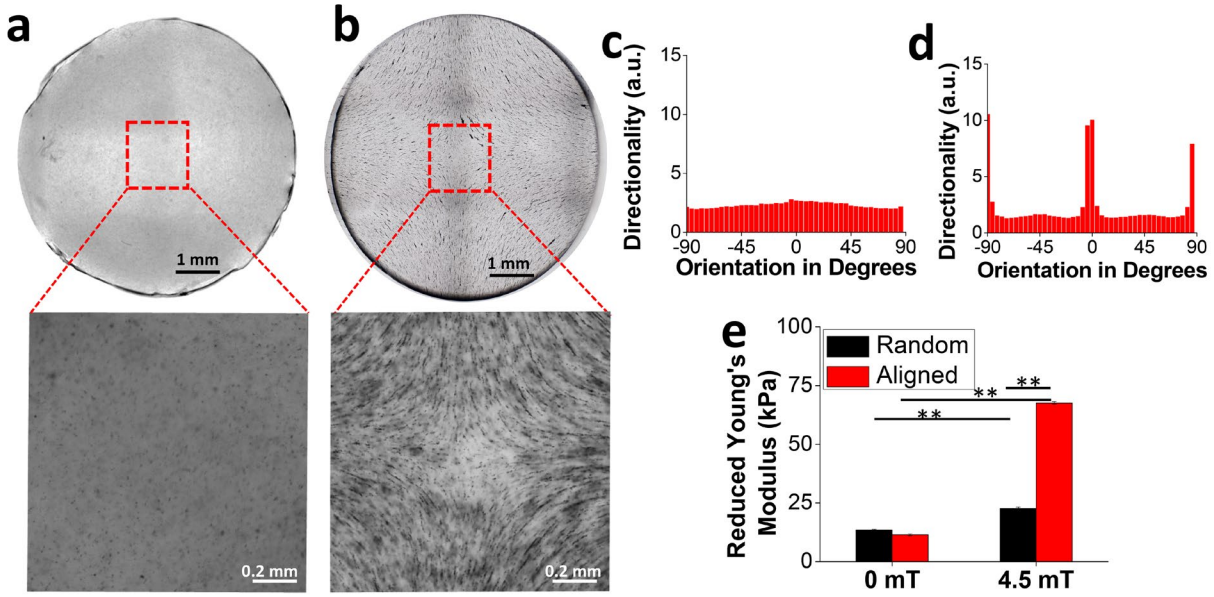

Figure 3. The pre-alignment of magnetic nanorods (MNRs) having a concentration of 20 µg/ml under the applied magnetic fields by the electromagnets with the same polarity. (a, b) Bright-field images of hydrogel with (a) randomly oriented MNRs or (b) pre-aligned MNRs. (c, d) MNR distribution was quantified by imaging analysis. (e) Modulus changes of randomly oriented and aligned MNRs under the applied magnetic fields (n = 5, * and ** denote statistical significance of $p < 0.05$ and $p < 0.01$, respectively).

To examine the effects of pre-aligned MNR concentration on hydrogel modulus change under the applied magnetic fields, hydrogel samples with various amounts of the pre-aligned MNRs were photo-crosslinked under UV light and then further subjected to various magnitudes of the applied magnetic fields. Furthermore, the effect of the magnetic polarities, either the same or opposite to the magnetic field applied during the pre-alignment, was investigated. As the concentration of NMR increased, the pattern of magnetic fields, visible from MNR alignment, became apparent (**Figure 4a-d**). As expected, the dynamic range of reduced Young's modulus increased as the MNR loading concentration increased **(Figure 4e-h)**. Specifically, the 3 μg/mL condition did not exhibit an appreciable change in modulus under any applied magnetic fields. The increase in the MNR loading concentration, however, not only increased the dynamic modulus range but also shortened the response time required to reach the stable modulus. Interestingly, the application of a magnetic field with the opposite polarity to the magnetic field applied during the pre-aligning induced less modulus change in all conditions (**Figure 4i-l**). These results demonstrate that our magneto-responsive hydrogel system with pre-aligned MNRs delivers almost 10 folds of modulus change from 10 kPa up to nearly 100 kPa, with a significantly less magnitude (under 4.5 mT) and application duration (20 mins) of magnetic fields, superior to other magneto-responsive systems.[13, 15] Based on our previous research, which determined the stem cell-relevant modulus range,[8a, 16] the 20 μg/mL condition was used in the rest of this study.

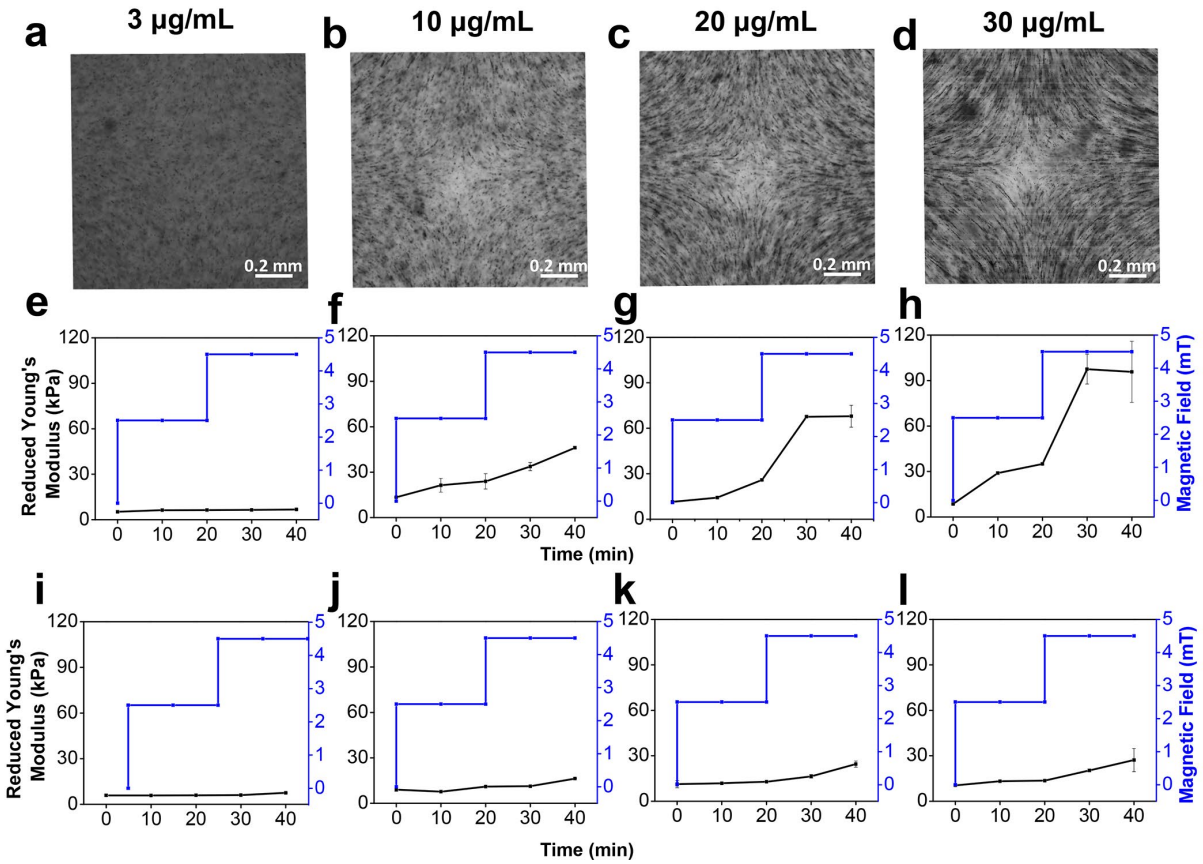

Figure 4. (a-d) Alignment pattern of the magnetic nanorods (MNRs) within the hydrogel having various concentrations. Modulus change of hydrogel depending on the loading concentration ((e, i) 3, (f, j) 10, (g, k) 20, and (h, l) 30 μg/mL) of pre-aligned MNRs and the polarity of the applied magnetic fields ((e-h) same polarity, (i-l) opposite polarity) with various magnitudes. The modulus was in-situ measured by atomic force microscopy. At least 5 samples were used for each MNR concentration and magnetic field polarity.

In order to verify the consistency of the modulus change throughout the entire hydrogel under magnetic fields with different polarities and magnitudes, the mechanical properties of the hydrogel at multiple locations were measured under the applied magnetic fields **(Figure 5)**. The samples were subjected to the stepwise magnitude and polarity changes of the applied magnetic fields, after pre-aligning MNRs and subsequent hydrogel UV crosslinking (**Figure 5a**). Corroborating with the previous results, the magnitude of the applied magnetic field was the predominant factor determining the modulus of the hydrogel. As expected from the distribution of MNRs within the hydrogel, the modulus change showed location-dependency; a similar, high increase in the reduced Young's modulus was observed in the regions with the MNRs oriented

toward the magnetic field (*i.e.*, points 2-5; approximately an average of 10 kPa - 70 kPa when 4.5 mT of the same polarity was applied) whereas the center of the hydrogel, point 1, experienced a less modulus change from approximately 10 kPa to 40 kPa under the same applied magnetic fields **(Figure 5b-f)**. This discrepancy is likely due to the relatively lower magnitude of magnetic fields exposed at the center location as shown in **Figure 2c**. These results indicate that the modulus change at a specific location within the hydrogel can be predicted by the magnetic field map, thus the local alignment of MNRs. Furthermore, the magneto-responsive hydrogel system was subjected to repeated cycles of stepwise magnetic field changes. The system demonstrated its superb repeatability over various stimulation regimens, showing its reversible capability, being able to stiffen and soften the hydrogel under dynamic magnetic polarities and field intensities **(Figure 5g)**. To test if the elasticity of the hydrogel down to its original modulus can be enhanced through the aid of applying the opposing polarity, two different conditions were monitored. One condition highlighted the relaxation time of the hydrogel to return to its original modulus after exposing it to a magnetic field of up to 4.5 mT and then removing the magnetic stimulus. As shown in **Figure 5h**, the hydrogel returned back to its original modulus of around 10 kPa in 80 minutes after the magnetic field was removed. In contrast, when the magnetic field stimulus was switched to the opposing polarity of 4.5 mT after the same polarity magnetic exposure, the hydrogel returned to its original modulus within only 10 mins **(Figure 5i)**. Further subjection of the opposite polarity beyond 10 mins, however, reversed the modulus change, slightly increasing it to the saturation value as shown in **Figure 4C**. The stiffening of hydrogel under both attractive and repulsive magnetic fields was further investigated by video-capturing the movements of pre-aligned MNRs under the applied magnetic fields. With the magnetic attraction, the outward movement of MNRs was clearly observed as shown in a time-lapse video (**Supplementary Video 1**) and its snap-shots with the feature tracking method (digital image correlation) in **Figure S1a, b**. This MNR movement would strain the hydrogel polymer fibers in localized areas, resulting in a modulus change. In comparison, magnetic repulsion caused the inward movement of MNRs (**Figure S1c, d**), also resulting in straining the hydrogel fibers albeit less degree.

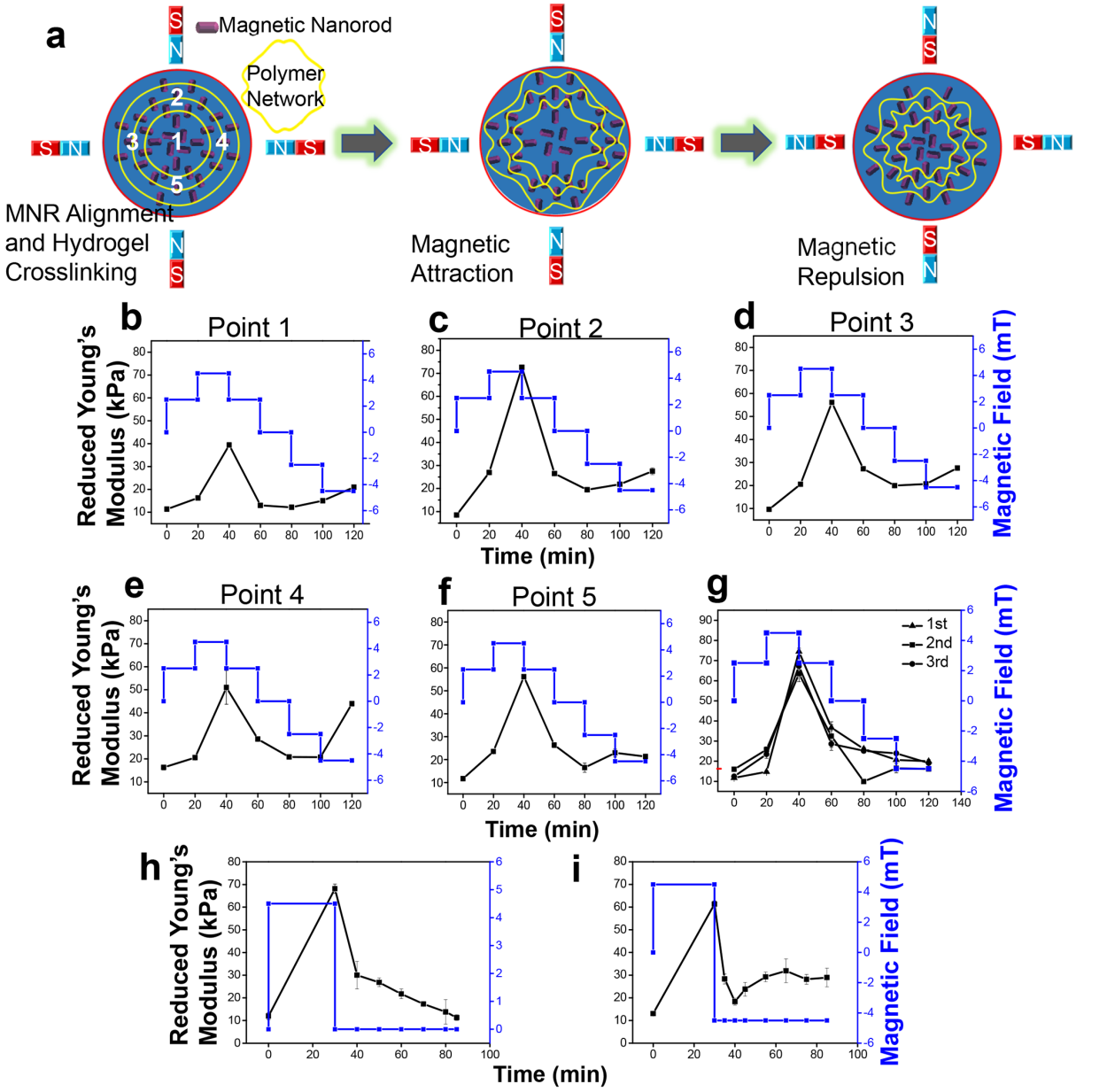

Figure 5. Local modulus change of magnetic nanorod (MNR)-incorporated hydrogel under various magnitudes and polarities of the applied magnetic fields. (a) Schematic showing the procedure of MNR pre-alignment/hydrogel crosslinking, and modulus measurements under the applied magnetic fields with the same polarity as the pre-aligning magnetic fields, followed by modulus measurements under the opposite polarity of the pre-aligning magnetic fields. (b-f) Changes in the modulus under various magnitudes and polarities of the applied magnetic fields at different locations of the hydrogel as shown in (a). (g) Reversibility and repeatability of modulus control in the hydrogel incorporated with pre-aligned MNRs. At least nine-point measurements from various areas on the hydrogel were used for the presented averages. (h) The relaxation duration of MNR-incorporated hydrogel was monitored by first subjecting

the system to a 4.5 mT magnetic field for 30 mins then the magnetic stimulus was removed while measuring modulus. (i) Facilitated relaxation duration of MNR-incorporated hydrogel was demonstrated by subjecting the system to a 4.5 mT magnetic field and then the polarity of the magnetic fields was switched to decrease the duration of the relaxation time. At least 5 samples for each condition or each point were used for the measurement of the modulus.

To further demonstrate the versatility of the hydrogel system to present anisotropic, yet predictable modulus changes in its local areas, three different magnetic field configurations were used, in which nine different points in the hydrogel were measured (**Figure 6a-c**). The configuration with the same polarity (to the pre-aligning magnetic fields) for all electromagnets, Configuration 1, induced the greatest change in modulus, where the sides nearest to the electromagnets (points 2-5) experienced greater modulus change at 50-70 kPa than Point 1, the middle region of the hydrogel at ~25 kPa (**Figure 6d**). The diagonal corners of the electromagnets (points 6-9) experienced a similar increase in modulus to those in points 2-5. In the second configuration, where the hydrogel was exposed to two different polarities, the top and bottom experienced the same polarity while the left and right regions experienced the opposite polarity at the same magnetic magnitude of 4.5 mT, generating an anisotropic modulus change (**Figure 6e**); the sides of the same polarity (*i.e.*, points 2 and 5) experienced a substantially increased modulus change, approximately at 50 kPa while the regions subjected to the opposite polarity (*i.e.*, points 3 and 4) experienced only a slight modulus increase, approximately at 20 kPa (**Figure 6e).** When the magnetic field polarity was switched (Configuration 3), a similar pattern of modulus change was observed, where the sides of magnetic fields with the same polarity as the pre-aligning magnetic field exhibited a greater modulus change than those with the opposite polarity in a predictable manner (**Figure 6f)**. These results demonstrate the capability of the system to apply an anisotropic, local modulus change in a predictable manner, enabling the subjection of individual cells to various magnitudes of modulus within a single cell culture.

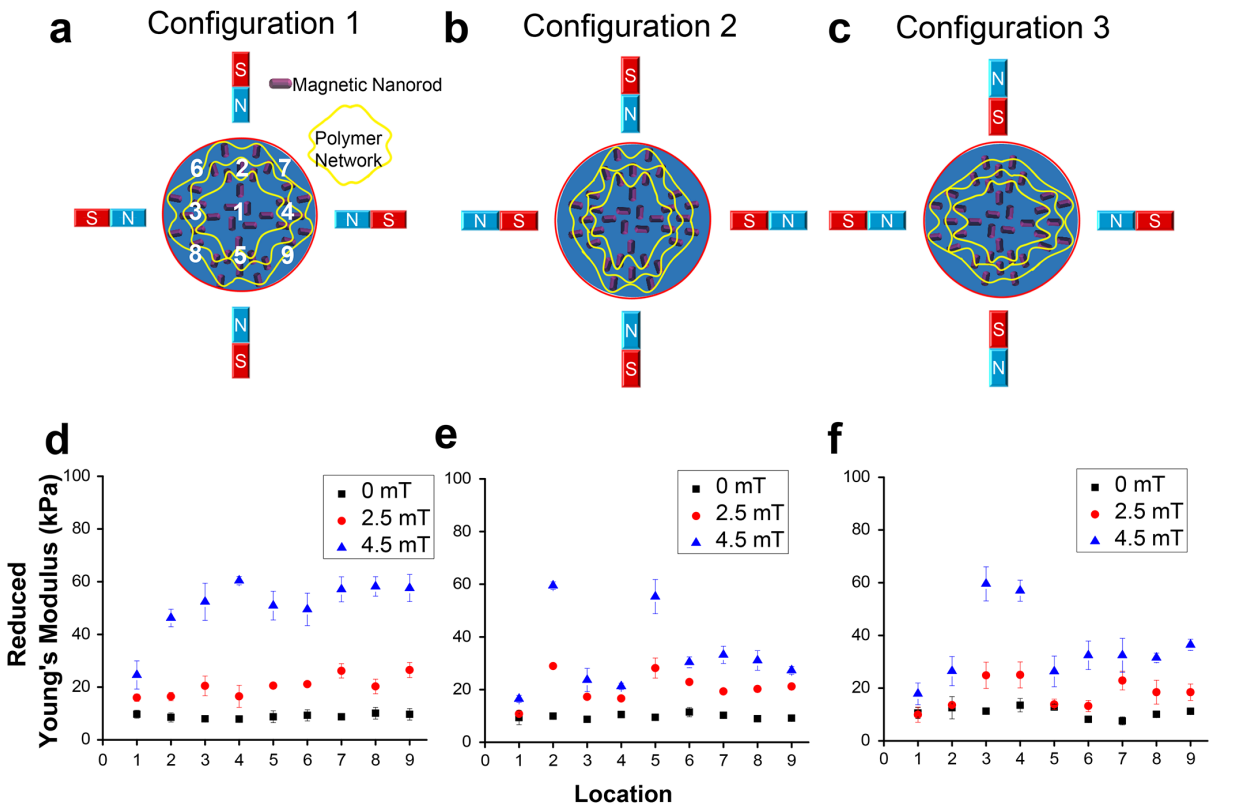

Figure 6. Heterogeneous modulus changes under different polarity configurations of the applied magnetic fields. Schematics showing different configurations of the applied magnetic fields and corresponding modulus measurements at various areas. (a) Same polarity (to the pre-aligning magnetic field) configuration (Configuration 1), (b) anisotropic polarity configuration (Configuration 2), and (c) alternative anisotropic polarity configuration (Configuration 3). (d-f) Corresponding location-dependent modulus changes in response to various polarity configuration ((d) Configuration 1, (e) Configuration 2 and (f) Configuration 3) and magnitude of the applied magnetic fields. At least 5 samples were used for each configuration.

In order to apply this magneto-responsive hydrogel system to biological applications, we examined the potential cytotoxicity of the GelMA incorporated with MNRs. Human iPSCs were inoculated in the hydrogel either with or without MNRs and the cell viability was determined using a live/dead cell assay for various culture durations (**Figure 7a**). There was no statistically significant negative effect of MNRs on cells as all conditions exhibited high cell viability above 90% (**Figure 7b**). It should be noted that the cells also formed spherical colonies with increasing size over the 7-day culture duration (**Figure 7a, c**), demonstrating a 3D culture system that provides a cellular microenvironment compatible with widely used Matrigel/Geltrex systems.[17]

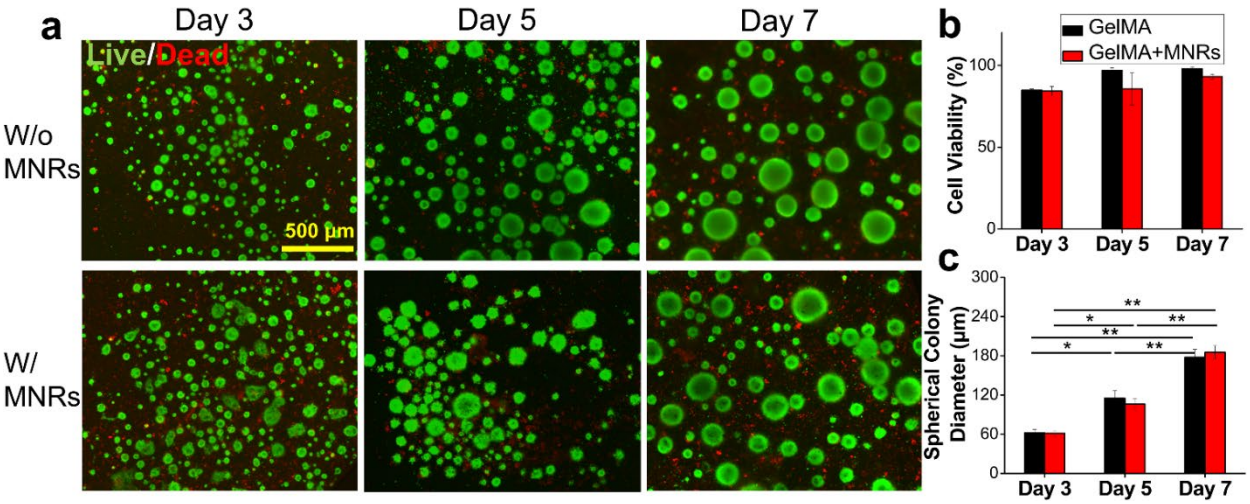

Figure 7. Cell viability in the MNR-incorporated hydrogel. (a) Representative live (green)/dead (red) cell assay images of human-induced pluripotent stem cells (iPSCs) cultured within 7.5 wt% gelatin methacrylate (GelMA) with or without MNRs for various durations (scale bar = 500 μm). (b) Quantitative analysis of cell viability in GelMA with or without the incorporation of MNRs. (c) Quantitative analysis of spherical cell colony diameter cultured in GelMA with or without the incorporation of MNRs (n = 5, * and ** denote statistical significance of $p < 0.05$ and $p < 0.01$, respectively).

To investigate the effects of MNR-induced hydrogel modulus control on stem cell behaviors, iPSCs were seeded into the hydrogel system and precultured for 5 days prior to being subjected to the applied magnetic fields. Applying a magnetic field at 4.5 mT without MNRs (control) did not induce the expression of Active-RhoA and YAP, both of which are mechano-sensitive signaling mediators (**Figure 8a, Figure S2a**). In contrast, iPSCs seeded with randomly oriented MNRs and subjected to two hours of 4.5 mT magnetic field after 5 days of pre-culture exhibited a slight increase of YAP and Active-RhoA expression on the outer regions of the colony (**Figure 8b, d, Figure S2b**). More significantly, the cells in the hydrogel with pre-aligned MNRs exhibited the greatest expression of active-RhoA and YAP expression under the same magnetic field (**Figure 8c, d, Figure S2c**), again demonstrating a superior dynamic range of the hydrogel with pre-aligned NMRs, which resulted in greater cellular responses.

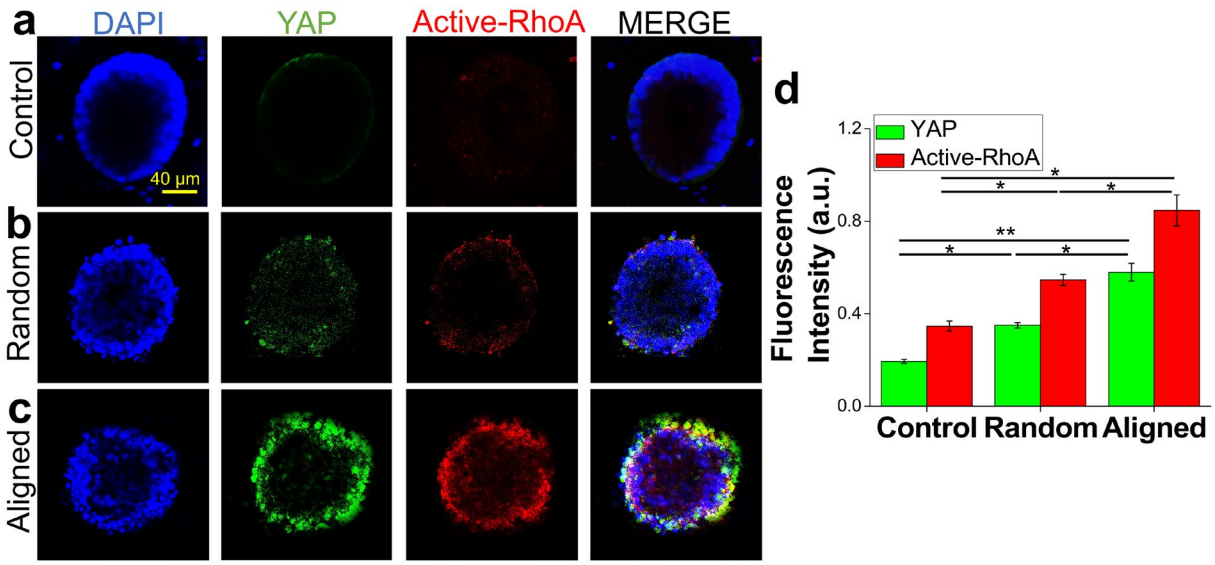

Figure 8. The effects of hydrogel stiffening on the mechano-sensitive RhoA signaling of human-induced pluripotent stem cells (iPSCs) cultured within MNR-incorporated hydrogel. Representative confocal images of the iPSC colonies in the hydrogel (a) without the incorporation of MNRs, (b) with randomly oriented MNRs, or (c) with pre-aligned MNRs, subjected to the applied magnetic field of 4.5 mT for 2 hours (scale bar = 40 μm). (d) Quantification of YAP and active-RhoA fluorescence intensities for various conditions (n = 5, * and ** denote statistical significance of $p < 0.05$ and $p < 0.01$, respectively).

Based on the results, which demonstrated the system's capability to generate a heterogeneous stiffness field within the individual hydrogel when exposed to anisotropic magnetic fields (**Figure 6**), the local modulus-dependent iPSC differentiation was investigated. Cells were inoculated into hydrogel with pre-aligned MNRs and pre-cultured for 5 days before being subjected to the anisotropic 4.5 mT magnetic field as shown in **Figure 6b**. Under the biochemical stimulation with BMP4 to induce simultaneous germ layer differentiation, the morphology of cell colonies significantly changed depending on the local hydrogel modulus. As shown in the 3D reconstructed images, while the iPSCs remained relatively spherical colony morphology in the absence of both MNRs and the applied magnetic field (Control), in the absence of MNRs but with the applied magnetic field (Control/Magnetic field) or the softer regions of the anisotropic condition, the cells formed a discoidal colony within the stiffer region of the hydrogel (**Figure 9a-d, Figure S3a-d**). The difference in the colony morphology was quantitatively assessed by measuring their sphericity, a degree of shape relative to the perfect sphere, through the 3D rendering of confocal images, showing the regional modulus-dependent

colony morphology under the same biochemical environment (**Figure 9e**). More interestingly, cells under the control, control/magnetic field, and softer conditions mainly expressed the ectodermal marker, SOX2, while a minimal expression of the mesendodermal marker expression, Brachyury (T), was observed (**Figure 9a-c, f**). In contrast, the migrating cells that are responsible for the colony morphology change in the stiffer region mainly expressed Brachyury (T), a mesendodermal marker, while SOX2, an ectodermal marker, was slightly expressed in the cells that were localized in the center of the colonies (**Figure 9d, f**). It should be noted that the modulus of the softer and stiffer regions remained relatively stable after 36 hours of anisotropic magnetic field exposure (**Figure S4**).

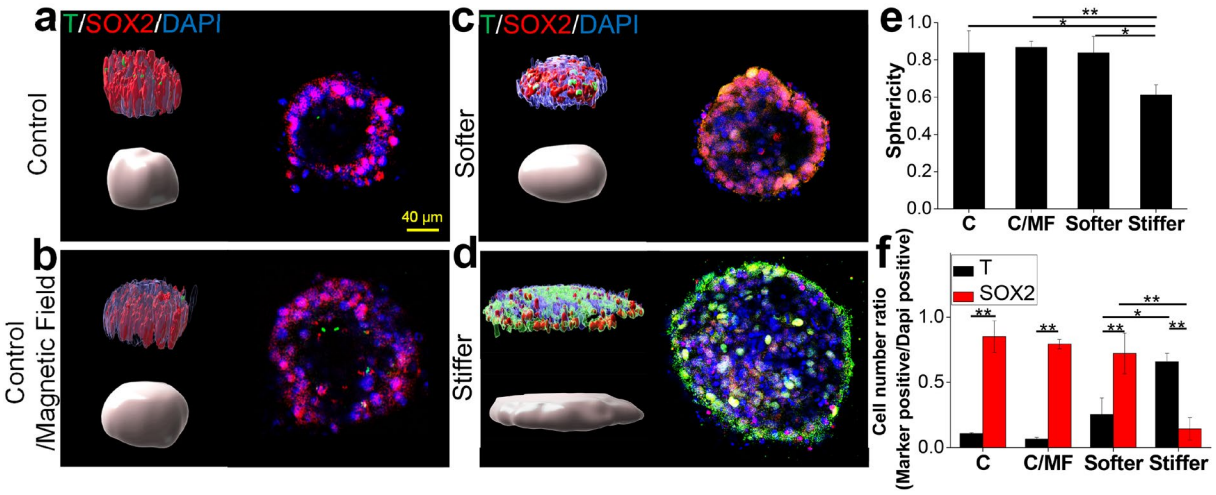

Figure 9. The effects of local modulus on the differentiation of human induced pluripotent stem cells (iPSCs). Representative confocal images of iPSC colony and its 3D reconstruction in (a) GelMA encapsulation without both MNR incorporation and magnetic field exposure (control), (b) GelMA encapsulation without MNR incorporation but with magnetic field exposure (control/magnetic field), (c) GelMA with both MNR incorporation and anisotropic magnetic field exposure at softer region (softer), or (d) GelMA with both MNR incorporation and anisotropic magnetic field exposure at stiffer region (stiffer). (e) Quantification of colony sphericity from the 3D reconstruction of iPSC colonies in the control, control/magnetic field, softer, and stiffer conditions. (f) Local modulus-dependent iPSC differentiation quantified from T^+ (mesendodermal marker) and $SOX2^+$ (ectodermal marker) cells in the 3D iPSC colony under various conditions (n = 5, * and ** denote statistical significance of $p < 0.05$ and $p < 0.01$, respectively, C: control, C/MF: control/magnetic field).

3. Discussion

In vivo, stem cells sense their niche and differentiate in accordance with their physicochemical microenvironment.[18] During the development, the ECM secreted from these differentiating cells and the forces from neighboring tissues dynamically alter their biomechanical environment, further stimulating the cells and guiding their tissue morphogenesis. To understand the role of mechanical factors on cellular behaviors, numerous studies have focused on statically controlling the physical microenvironment by utilizing scaffolds of different elastic moduli or unidirectionally stiffening or softening hydrogels via a time-dependent increase or decrease in crosslinking density.[8a, 19] Although these systems have provided excellent platforms to study mechanobiology, they often fail to capture the dynamic nature of *in vivo* microenvironment, especially during tissue morphogenesis. One approach to dynamically control matrix stiffness utilizes the hydrogel with reversible mechanics by in-situ control over crosslinking density.[10, 20] This approach requires exogenous chemical (e.g., Ca^{2+}) or physical (UV/NIR) stimuli to control the interaction among hydrogel polymer networks, hence its stiffness, but such stimuli may also directly affect cells through Ca^{2+} signaling and heat shock proteins.[21] Another approach utilizes the magneto-responsiveness of MNPs embedded within the hydrogel.[12b, 15] However, these systems require substantial magnitudes of magnetic fields in the range of hundreds of mT, likely causing heat generation issues when magnetic generators (e.g., electromagnet) are used to dynamically regulate magnetic fields.

To address the shortcoming of MNP-based systems requiring high magnetic fields for cell-relevant stiffness control, we utilized two separate yet collaborating approaches. The mechanism underlying the MNP-induced stiffening of the hydrogel is based on the microscopic movement of the MNPs, straining the polymeric fibers of the hydrogel in response to the magnetic stimuli. Instead of spherical MNPs (MNSs), we employed a rod shape of MNPs (MNRs); since MNRs have a clear polarity with respect to the length of the particle, changing the polarity of a magnetic field causes MNRs to rotate in addition to their translational motion, exerting greater strains to the surroundings in comparison to MNSs as demonstrated in our previous study.[22] Furthermore, this magnetic anisotropy in MNRs allows alignment of the particles according to a magnetic field, providing an opportunity to maximize the magneto-responsiveness of the system; the pre-alignment of MNRs before hydrogel crosslinking resulted in a more than 500% increase in the dynamic modulus range as compared to that of randomly

oriented MNRs within the hydrogel, likely by avoiding the canceling effect of random orientation. This improvement in the magneto-responsiveness in our system significantly reduced the required magnitudes of magnetic fields from hundreds of mT to several mT[12b, 15, 23] for the dynamic range of modulus to cover the physiologically relevant stiffness to direct diverse cellular responses. The response time of the system is also substantially enhanced as the modulus change was stabilized within minutes of magnetic field application as compared to the hours required to reach the maximum modulus change in other systems.[13]

The pre-alignment of MNRs also enables faster reversible change in modulus and its anisotropic distribution within the same hydrogel in a predictable manner. As demonstrated in the disproportional modulus change under various configurations of electromagnets, the movement of the MNRs within the hydrogel, hence straining of the hydrogel polymeric network is influenced by the polarity as well as the magnitude of the magnetic field. As shown in the response under a stepwise magnetic field stimulation, removal of the magnetic field does not result in the immediate recovery of the original hydrogel modulus, likely due to the viscoelastic nature of the hydrogel. The application of the magnetic field in the opposite polarity, however, readily changes the hydrogel modulus to the original state. Further exposure of the opposite polarity, interestingly, caused the increase of the hydrogel modulus. The increase of the stiffness under the opposite polarity (repulsive), however, was less than that under the same polarity (attractive) of the magnetic field. This was consistent with the observation of MNR movement under magnetic fields (**Figure S1)**, where the movement distance of the MNRs under the repulsive magnetic field is shorter than that under the attractive magnetic field, leading to a less amount of polymeric chain straining, thus a less increase of the modulus. This difference in moving distance is likely due to the distance-dependent magnetic field intensity from the electromagnets, where the farther the distance from the magnet (the closer to the center), the lower the magnetic field. Under the attractive magnetic field, the MNRs were attracted towards the electromagnets, receiving a stronger magnetic field and a stronger attractive force, resulting in a longer movement distance and straining the fibers more. In contrast, under the repulsive magnetic field, the MNRs were pushed away from the electromagnets, receiving a weaker magnetic field and a weaker repulsive force, resulting in a shorter movement distance and straining the fibers less. Such a translational movement of MNRs, regardless of the direction, has been shown to exert an internal force on the hydrogel fiber network for its stiffening response as

demonstrated by Chen et al.[15] The local concentration change of MNRs could have an effect on the modulus change but its effect appears minimal based on the fact that 1) an insignificant difference of hydrogel modulus was observed when the concentration of MNRs was varied under no magnetic field, and 2) the center of the construct exhibited a modulus increase even under the attractive magnetic field, which would reduce the local MNR concentration. Based on the location-specific heterogeneous modulus response under the anisotropic polarities of the applied magnetic fields, we also demonstrated the generation of variable modulus fields within the monolithic hydrogel. The local modulus of the hydrogel was precisely controlled resulting in the regions that were exposed to the same polarity to the pre-aligning magnetic field experiencing the highest change in modulus in comparison to regions under the opposing magnetic field polarity. These results demonstrate the potential use of the magneto-responsive hydrogel for mechanobiology studies where the mechanical factor can be decoupled from other physicochemical factors by culturing the cells in the same biochemical conditions yet in a different local mechanical environment.

The feasibility of the system for mechanobiology study was demonstrated by investigating both a short-term cellular response and a long-term iPSC differentiation. Among various mechano-responsive signaling cascades, the RhoA signaling pathway has been shown to be vital in determining stem cell fate.[24] The RhoA signaling drives cytoskeletal remodeling and regulates gene expression in response to the mechanical change in the microenvironment (e.g., change in substrate stiffness) leading to lineage specification.[25] YAP is also a mechano-mediator that is significantly involved in embryo development.[26] iPSCs cultured in the hydrogel without MNRs or not subjected to magnetic fields did not exhibit RhoA and YAP signaling activation. In contrast, iPSCs that were inoculated within the hydrogel with both randomly oriented or aligned MNRs, under magnetic stimulation, exhibited RhoA and YAP activation. The aligned MNR condition, however, showed greater expression of these mechano-sensitive markers. Due to the dynamic stiffening, the RhoA signaling pathway was activated in which the actin-myosin bundles reciprocated to compensate for the change in the physical microenvironment, hence leading to the activation of YAP.[27] We also showed modulus-dependent differentiation of iPSCs by applying anisotropic magnetic fields to create a gradient of modulus field within the hydrogel. Colonies positioned in the stiffer regions exhibited the migration of T^+ cells, similar to that observed during embryo development. In contrast, colonies

in the softer regions exhibited a more spherical morphology with greater SOX2 expression. Previous studies have shown how the mechanical/physical niche can affect iPSC dimensionality and differentiation patterns, where greater expression of mesendodermal markers was observed in the iPSC colonies on stiffer scaffolds as compared to softer scaffolds that induced greater ectodermal differentiation.[8a] Furthermore, compared to previous 2D culture systems where cells were typically seeded on top of the hydrogel surface, our magneto-responsive hydrogel system enabled the 3D culture of iPSCs where the 3D microenvironment can be more precisely controlled to mimic *in vivo* conditions.[12c] The results from the current study demonstrate that our magneto-responsive hydrogel system with pre-aligned MNRs can produce a monolithic culture platform with a controlled gradient of hydrogel modulus in 3D, providing a means to subject cells to diverse mechanical microenvironment under otherwise identical culture conditions.

4. Conclusion

Overall, the GelMA hybrid hydrogels incorporated with MNRs show a strong mechanical response to low-intensity magnetic fields. By using the nanorod's ferromagnetic properties, the pre-alignment of MNRs prior to hydrogel crosslinking not only further enhances the dynamic range but also enables the generation of a modulus gradient in a location-specific manner. The feasibility of the system in mechanobiology studies is demonstrated by the activation of the mechano-sensitive RhoA and YAP signaling pathways, indicating that the magneto-responsive hydrogel can dynamically control hydrogel modulus in a stem cell-relevant range. Therefore, the presented magneto-responsive hydrogel system offers a facile means to dynamically modulate the mechanical microenvironment of stem cells to induce local modulus-dependent cellular responses within the same substrate. Collectively, these results demonstrate the versatility and reliability of the magneto-responsive hydrogel system as an excellent platform for investigating the mechanobiology of various cells/tissues for the discovery/development of potential therapeutics.

5. Experimental Section

Magnetic Fe_3O_4-SiO_2 Nanorod (MNR) synthesis: The FeOOH nanorods, having a length of approximately 2 μm, were firstly synthesized using a hydrothermal method as described elsewhere.[12c, 22, 28] Briefly, 19.464 g of iron chloride ($FeCl_3$, Sigma) was dissolved in 200 mL of

deionized (DI) water. The solution was placed in an oven at 98 °C for 24 h. The obtained FeOOH nanorods were washed three times and redispersed in 160 mL of DI water. For the SiO_2 encapsulation of the nanorods, FeOOH nanorods were first modified by polyacrylic acid (PAA, Sigma); 40 mL of PAA (0.1 M) was added to the above solution and stirred overnight. The samples were centrifuged and redispersed in 50 mL DI water. Silica coating on FeOOH was then achieved by injecting 40 μL of tetraethyl orthosilicate (TEOS, Sigma) into a mixture containing 20 mL of ethanol, 1.5 mL of DI water, 0.5 mL of above FeOOH solution, and 1 mL of ammonium hydroxide ($NH_3 \cdot H_2O$, Fisher). After sonication for 30 minutes, the FeOOH-SiO_2 was collected by centrifuge and washed with ethanol and DI water. Fe_3O_4 MNRs were synthesized by reducing FeOOH-SiO_2 nanorods at high calcination temperatures; FeOOH-SiO_2 nanorods were dried in crucibles and placed in a tubular furnace. The reduction occurred at 360 °C for 2 hours. After cooling down to room temperature, the prepared MNRs were washed with DI water three times. As a comparison to the MNRs, magnetic Fe_3O_4-SiO_2 nanospheres, having a diameter of approximately 450 nm, were synthesized according to a previous study.[29] Briefly, 0.6 g of poly(4-styrenesulfonic acid-co-maleic acid, SS:MA = 3:1) sodium salt (PSSMA (3:1), Sigma) and 0.325 g of $FeCl_3$ were added to the mixture containing 39.6 mL of ethylene glycol (Sigma) and 0.4 mL of water. After stirring for 15 min, 1.026 g of sodium acetate (Sigma) was added to the mixture and stirred for another 15 min. The obtained solution was transferred to a Teflon-lined stainless-steel autoclave (100 mL) and reacted at 200 °C for 10 h. After cooling to room temperature, the product was washed with ethanol and water and dispersed in 20 mL of water. The silica coating was applied to the nanospheres using the same method as described above.

GelMA Synthesis: For the hydrogel preparation, 4 g of type A porcine skin gelatin was dissolved in 40 mL Dulbecco's phosphate buffered saline (DPBS; GIBCO) at 60 °C and stirred until fully dissolved.[30] 3 mL of methacrylic anhydride (Sigma) was then added, at a rate of 0.5 mL/min, to the gelatin solution under stirring conditions at 50 °C and the mixture was allowed to react for 1hr. The reaction was terminated by adding 120 mL DPBS and the mixture was then dialyzed for 5 days to remove any unreacted methacrylic anhydride or acrylic acid byproduct. The polymer solution was lyophilized for 7 days. The GelMA precursor solution was prepared by dissolving a certain amount of GelMA in the DPBS, having 0.05% of a photoinitiator, lithium phenyl-2,4,6-trimethylbenzoylphosphinate (LAP).

MNR alignment and encapsulation: To incorporate MNR into the GelMA hydrogel, various concentrations of MNRs in GelMA precursors were used. 1 mL of 7.5 wt% GelMA precursor was placed into a 1.5 mL microcentrifuge tube while mixing with 3, 10, 20, or 30 μg of MNRs. The GelMA/MNR precursor solution was sonicated at 37 °C for 1 min to prevent MNR aggregation. To align the MNRs within the GelMA precursor, 40 μL of the GelMA/MNR precursor solution was pipetted into a PDMS mold, having a cylindrical well of 6 mm in diameter and 1 mm in depth, and was then placed at the center of four 12 V DC electromagnets (McMASTER-CARR). The four electromagnets were orthogonally placed around the hydrogel and the distance between two face-to-face electromagnets was 5 cm. 7.5 mT of the magnetic field, generated by the four electromagnets with north polar facing inwards (same polarity), was applied to the GelMA/MNR precursor solution for 5 minutes. The precursor was then crosslinked using a UV light for 90 s. The GelMA precursor without aligned MNRs was also crosslinked as a control group. Magnetic field intensities were measured using a Gauss meter (HT20, Resolution: 1 mT) on the surface of the electromagnets.

Mechanical Characterization of MNR incorporated hydrogel under magnetic field: The reduced Young's modulus of the randomly oriented or aligned MNR hydrogel with different MNR concentrations under various magnitudes/polarities of the applied magnetic fields was measured using the MFP-3D AFM (Asylum Research). Briefly, a modified silicon nitride tip (spring constant: 0.6 N/m) attached with a 20 μm diameter borosilicate sphere (indenter's diameter) was used to generate load-indentation depth curves. Hertz model was used to calculate the Reduced Young's modulus E^* as described below:

$E^* = \frac{3}{4} \cdot R^{-\frac{1}{2}} \cdot h^{-\frac{3}{2}} \cdot P \cdot Z$,[31]

, where R is the indenter's radius, h is the indentation depth, P is the load, and Z is the correction factor.

iPSC culture in MNR-incorporated hydrogel: A well-characterized human iPSC cell line[8a, 16] was maintained on Geltrex-coated tissue culture polystyrene plates in mTeSR™ 1 medium (Stemcell Technologies, Vancouver, Canada) in a humidified incubator at 37 °C and 5% CO_2 prior to their inoculation into the MNR-incorporated hydrogel. The cells were detached from the culture plates using Accutase (Fisher) and mixed with the hydrogel precursor solution of 15 wt% of GelMA precursor to achieve 2 million cells per mL. 40 μL of cell/GelMA precursor solution was mixed with 0.8 μg of MNRs (20 μg/mL) and pipetted into the previously mentioned PDMS mold in a petri dish in which the final GelMA concentration was 7.5 wt%. The precursor was then photo-crosslinked for 90 s under UV light exposure either with or without pre-aligning the NMRs as previously described. 10 μM of Y-27632 (Sigma) was added during the first 24 hours of culture duration to enhance the cell viability.
After 5 days of the pre-culture period, the cell/GelMA complex having non-aligned or aligned MNRs (20 μg/mL) was exposed to 4.5 mT of magnetic field for 1 hour before being fixed with 4% paraformaldehyde (PFA, Fisher). The cells encapsulated within the hydrogel without any MNR were also fixed and used as a control. To examine iPSC differentiation behavior within the hydrogel of anisotropic modulus, iPSCs were pre-cultured for 5 days and then treated with BMP4 (40 ng mL^{-1}) for 36 hours while applying a magnetic field of 4.5 mT (same polarity as pre-alignment) for the entire duration of the 36-hour differentiation to induce simultaneous germ layer differentiation. Differentiated 3D iPSC colonies were fixed using 4% paraformaldehyde.

iPSC Viability assessment: Viability for cells encapsulated in 7.5 wt% GelMA and the hydrogel with MNRs were assessed through a live/dead cell assay (Invitrogen). Cells were cultured for 3, 5, and 7 days before the viability assay. The cells were stained with 0.5 μl/mL of calcein AM and 2 μl/mL of ethidium homodimer-1 (EthD-1) in DPBS for 5 mins at room temperature. Fluorescent image acquisition was carried out using a Nikon-Eclipse TI microscope (Nikon). Cell viability % was evaluated using the ImageJ software.

Immunofluorescence confocal imaging: Samples were immuno-stained following a standard immunofluorescence staining protocol. Briefly, the fixed samples were permeabilized by 0.1% Triton-X in a phosphate-buffered saline (PBS) followed by blocking of non-specific binding sites with 1% bovine serum albumin (BSA) in PBS. The following antibodies were utilized for the detection of specific protein expression: rabbit anti-YAP (Cell Signaling), mouse anti-Active RhoA-GTP (NewEast Biosciences), goat anti-BRACHYURY (R&D Systems), rabbit anti-SOX2

(Cell Signaling) and appropriate secondary antibodies. The samples were then counter-stained with 4′,6-diamidino-2-phenylindole (DAPI, Sigma) to visualize the nuclei. Z stack images with 1 μm interval were taken using a Zeiss 880 confocal microscope.

Image analysis: Imaris 7.1.1 (Bitplane) was used to analyze the colony morphology of iPSCs from confocal imaging to measure the sphericity (*i.e.*, the ratio of the surface area of a sphere to the surface area of the object).[8a, 16a]

Statistical Analysis: All experiments were conducted with a minimum of triplicate biological samples and data are represented as mean ± standard deviation (SD). Comparison of groups for statistical significance was determined using SPSS 15 software with one-way ANOVA analysis with Tukey's posthoc.

Supporting Information

Supporting information is available from the Wiley Online Library.

Acknowledgements

This work was supported by UC Riverside and Korea Institute of Materials Science (Research Program PNK7280) through UC-KIMS Center for Innovative Materials for Energy and Environment.

Received: ((will be filled in by the editorial staff))

Revised: ((will be filled in by the editorial staff))

Published online: ((will be filled in by the editorial staff))

[1] a) A. J. Bloor, A. Patel, J. E. Griffin, M. H. Gilleece, R. Radia, D. T. Yeung, D. Drier, L. S. Larson, G. I. Uenishi, D. Hei, *Nature Medicine* **2020**, 26 (11), 1720; b) H. Gu, X. Huang, J. Xu, L. Song, S. Liu, X.-b. Zhang, W. Yuan, Y. Li, *Stem Cell Research & Therapy* **2018**, 9 (1), 1; c) Y.-T. Tan, L. Ye, F. Xie, A. I. Beyer, M. O. Muench, J. Wang, Z. Chen, H. Liu, S.-J. Chen, Y. W. Kan, *Proceedings of the National Academy of Sciences* **2018**, 115 (9), 2180.

[2] A. Sharma, S. Sances, M. J. Workman, C. N. Svendsen, *Cell stem cell* **2020**, 26 (3), 309.

[3] a) J. Xu, J. G. Shamul, N. A. Staten, A. M. White, B. Jiang, X. He, *Small* **2021**, 17 (33), e2102219; b) Y. Ma, M. Lin, G. Huang, Y. Li, S. Wang, G. Bai, T. J. Lu, F. Xu, *Advanced Materials* **2018**, 30 (49), 1705911; c) B. Lloyd-Lewis, P. Mourikis, S. Fre, *Current opinion in cell biology* **2019**, 61, 16; d) W. B. Swanson, M. Omi, Z. Zhang, H. K. Nam, Y. Jung, G. Wang, P. X. Ma, N. E. Hatch, Y. Mishina, *Biomaterials* **2021**, 272, 120769.

[4] a) J.-L. Maître, H. Turlier, R. Illukkumbura, B. Eismann, R. Niwayama, F. Nédélec, T. Hiiragi, *Nature* **2016**, 536 (7616), 344; b) J. M. Muncie, N. M. Ayad, J. N. Lakins, X. Xue, J. Fu, V. M. Weaver, *Developmental cell* **2020**, 55 (6), 679.

[5] B. K. Hall, S. Herring, *Journal of morphology* **1990**, 206 (1), 45.

[6] a) J. M. Barnes, L. Przybyla, V. M. Weaver, *Journal of cell science* **2017**, 130 (1), 71; b) B. L. Roman, K. Pekkan, *Biomechanics and modeling in mechanobiology* **2012**, 11 (8), 1149; c) T. Haack, S. Abdelilah-Seyfried, *Development* **2016**, 143 (3), 373.

[7] J. Voog, D. L. Jones, *Cell stem cell* **2010**, 6 (2), 103.

[8] a) M. Maldonado, G. Ico, K. Low, R. J. Luu, J. Nam, *Advanced healthcare materials* **2016**, 5 (12), 1408; b) Y. Zhu, X. Li, R. R. R. Janairo, G. Kwong, A. D. Tsou, J. S. Chu, A. Wang, J. Yu, D. Wang, S. Li, *Journal of Cellular Physiology* **2019**, 234 (5), 7569; c) C. Kim, J. L. Young, A. W. Holle, K. Jeong, L. G. Major, J. H. Jeong, Z. M. Aman, D.-W. Han, Y. Hwang, J. P. Spatz, *Annals of biomedical engineering* **2020**, 48 (2), 893; d) W. J. Hadden, J. L. Young, A. W. Holle, M. L. McFetridge, D. Y. Kim, P. Wijesinghe, H. Taylor-Weiner, J. H. Wen, A. R. Lee, K. Bieback, *Proceedings of the National Academy of Sciences* **2017**, 114 (22), 5647.

[9] A. M. Rosales, K. S. Anseth, *Nature Reviews Materials* **2016**, 1 (2), 1.

[10] O. Jeon, T.-H. Kim, E. Alsberg, *Acta Biomaterialia* **2021**, 136, 88.

[11] S. Hackelbusch, T. Rossow, D. Steinhilber, D. A. Weitz, S. Seiffert, *Advanced Healthcare Materials* **2015**, 4 (12), 1841.

[12] a) F. A. Blyakhman, G. Y. Melnikov, E. B. Makarova, F. A. Fadeyev, D. V. Sedneva-Lugovets, P. A. Shabadrov, S. O. Volchkov, K. R. Mekhdieva, A. P. Safronov, S. Fernández Armas, *Nanomaterials* **2020**, 10 (9), 1697; b) K. A. Tran, E. Kraus, A. T. Clark, A. Bennett, K. Pogoda, X. Cheng, A. Cēbers, P. A. Janmey, P. A. Galie, *ACS applied materials & interfaces* **2021**, 13 (18), 20947; c) A. A. Abdeen, J. Lee, N. A. Bharadwaj, R. H. Ewoldt, K. A. Kilian, *Advanced healthcare materials* **2016**, 5 (19), 2536.

[13] T. Yan, D. Rao, Y. Chen, Y. Wang, Q. Zhang, S. Wu, *Acta Biomaterialia* **2022**, 138, 112.

[14] D. Nguyen, T. Long, X. Jia, W. Lu, X. Gu, Z. Iqbal, S. Jiang, *Scientific reports* **2019**, 9 (1), 1.

[15] W. Chen, Y. Zhang, J. Kumari, H. Engelkamp, P. H. Kouwer, *Nano letters* **2021**, 21 (16), 6740.

[16] a) M. Maldonado, L. Y. Wong, C. Echeverria, G. Ico, K. Low, T. Fujimoto, J. K. Johnson, J. Nam, *Biomaterials* **2015**, 50, 10; b) M. Maldonado, R. J. Luu, G. Ico, A. Ospina, D. Myung, H. P. Shih, J. Nam, *Stem cell research & therapy* **2017**, 8 (1), 1.
[17] M. Hofer, M. P. Lutolf, *Nature Reviews Materials* **2021**, 6 (5), 402.
[18] C. A. Chacón-Martínez, J. Koester, S. A. Wickström, *Development* **2018**, 145 (15), dev165399.
[19] a) M. Guvendiren, J. A. Burdick, *Nature communications* **2012**, 3 (1), 1; b) S. R. Caliari, M. Perepelyuk, E. M. Soulas, G. Y. Lee, R. G. Wells, J. A. Burdick, *Integrative Biology* **2016**, 8 (6), 720.
[20] a) J. V. Accardo, J. A. Kalow, *Chemical Science* **2018**, 9 (27), 5987; b) M. R. Arkenberg, D. M. Moore, C.-C. Lin, *Acta biomaterialia* **2019**, 83, 83; c) Z. Zheng, J. Hu, H. Wang, J. Huang, Y. Yu, Q. Zhang, Y. Cheng, *ACS applied materials & interfaces* **2017**, 9 (29), 24511.
[21] a) C. Shimoni, M. Goldstein, I. Ribarski-Chorev, I. Schauten, D. Nir, C. Strauss, S. Schlesinger, *Frontiers in cell and developmental biology* **2020**, 956; b) S. K. Wu, G. A. Gomez, S. J. Stehbens, M. Smutny, *Frontiers in Cell and Developmental Biology* **2020**, 8, 960; c) H. W. Snoeck, *EMBO reports* **2020**, 21 (6), e50028.
[22] S. Kim, G. Ico, Y. Bai, S. Yang, J.-H. Lee, Y. Yin, N. V. Myung, J. Nam, *Nanoscale* **2019**, 11 (43), 20527.
[23] E. A. Corbin, A. Vite, E. G. Peyster, M. Bhoopalam, J. Brandimarto, X. Wang, A. I. Bennett, A. T. Clark, X. Cheng, K. T. Turner, *ACS applied materials & interfaces* **2019**, 11 (23), 20603.
[24] Z. Zhang, M. Liu, Y. Zheng, *Biochemical Society Transactions* **2021**, 49 (6), 2941.
[25] R. McBeath, D. M. Pirone, C. M. Nelson, K. Bhadriraju, C. S. Chen, *Developmental cell* **2004**, 6 (4), 483.
[26] J. R. Davis, N. Tapon, *Development* **2019**, 146 (18), dev167106.
[27] G. Halder, S. Dupont, S. Piccolo, *Nat Rev Mol Cell Biol* **2012**, 13 (9), 591.
[28] a) M. S. Wang, L. He, S. Zorba, Y. D. Yin, *Nano Letters* **2014**, 14 (7), 3966; b) Z. W. Li, C. Qian, W. J. Xu, C. H. Zhu, Y. D. Yin, *Sci Adv* **2021**, 7 (37).
[29] J. Ge, Y. Hu, M. Biasini, W. P. Beyermann, Y. Yin, *Angewandte Chemie International Edition* **2007**, 46 (23), 4342.
[30] T. Jariwala, G. Ico, Y. Tai, H. Park, N. V. Myung, J. Nam, *ACS Applied Bio Materials* **2021**, 4 (4), 3706.
[31] a) S. Kontomaris, A. Malamou, *Materials Research Express* **2020**, 7 (3), 033001; b) S.-V. Kontomaris, A. Malamou, *Materials Research Express* **2018**, 5 (12), 125403.